Peer-reviewed version available at *Sensors* **2019**, *20*, 145; doi:10.3390/s20010145

Article

Performance-Enhanced Non-Enzymatic Glucose Sensor Based on Graphene-Heterostructure

Mahmoud A. Sakr[1,2], Karim Elgammal[3,5], Anna Delin[3,4,5], Mohamed Serry[2,*]

[1] Graduate Program in Nanotechnology, The American University in Cairo (AUC), New Cairo, 11835, Egypt
[2] Department of Mechanical Engineering, The American University in Cairo (AUC), New Cairo, 11835, Egypt
[3] Department of Applied Physics, School of Engineering Sciences, KTH Royal Institute of Technology, Electrum 229, SE-16440 Kista, Sweden
[4] Department of Physics and Astronomy, Materials Theory Division, Uppsala University, Box 516, SE-75120 Uppsala, Sweden
[5] Swedish e-Science Research Center (SeRC), KTH Royal Institute of Technology, SE-10044 Stockholm, Sweden
* Corresponding author: Email: mserry@aucegypt.edu, Tel: +202-2615-3098

Abstract: Non-enzymatic glucose sensing is a crucial field of study because of the current market demand. This study proposes a novel design of glucose sensor with enhanced selectivity and sensitivity by using graphene Schottky diodes, which is composed of Graphene/Platinum Oxide/n-Silicon heterostructure. The sensor was tested with different glucose concentrations and interfering solutions to investigate its sensitivity and selectivity. Different structures of the device were studied by adjusting the platinum oxide film thickness to investigate its catalytic activity. It was found that the film thickness plays a significant role in the efficiency of glucose oxidation and hence in overall device sensitivity. Moreover, theoretical investigations were conducted using Density Function Theory (DFT) to better understand the detection method and the origins of selectivity. The working principle of the sensors puts it in a competitive position with other non-enzymatic glucose sensors. DFT calculations provided a qualitative explanation of the charges distributed across the graphene sheet within a system of a platinum substrate with D-glucose molecules above. The proposed graphene/PtO/n-Si heterostructure has proven to satisfy these factors, which opens the door for further developments of more reliable non-enzymatic glucometers for continuous glucose monitoring systems.

Keywords: Graphene; Electrochemical, Biosensor, Heterostructure, Non-Enzymatic; Schottky Diode, Glucose, Glucometers, ALD, PtO

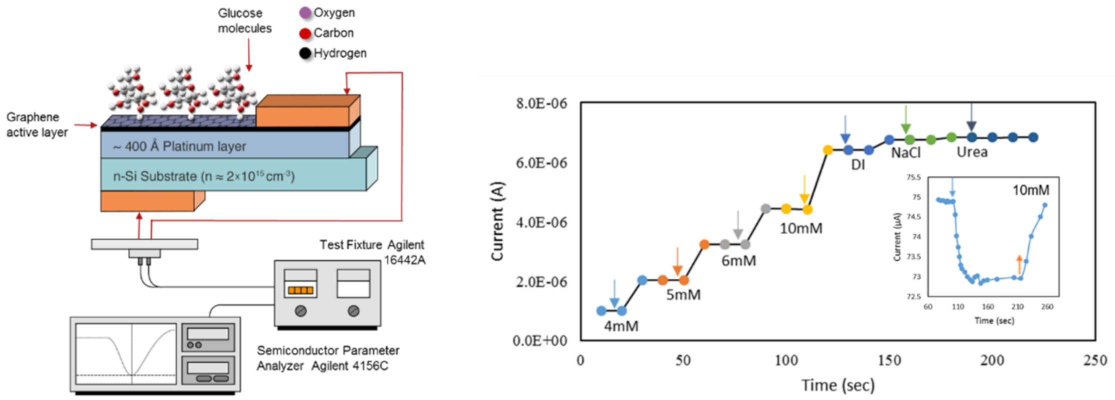

(a) (b)

Graphical Abstract

1. Introduction

Electrochemical biosensors work through the perception of a chemical reaction that takes place between an electrode and the bio-analyte of interest to transduce an electrical signal. Thus, they consist of two main elements; a biological sensing probe (i.e., recognition elements) and a transducer. For the latter, amperometry, voltammetry, and electrochemical impedance spectroscopy (EIS) are the most common transduction methods in electrochemical biosensors, in which detection is based on either electron-transfer rate, background current, or accumulation of analytes.

Since its inception in 1964 [1], electrochemical biosensing has been the most widely researched and commercialized method for blood glucose and bio-analyte monitoring. Their primary advantages over other biosensing methods (e.g., optical, thermal, and FET biosensors) are their ease of fabrication and their ability to detect bio-analytes without interfering with the biological system. The advance of electrochemical biosensing has leaped since the introduction of nanomaterials and bioMEMS in the late 1990s which stimulated enhancing electrochemical biosensing performance (e.g. detection limit, sensitivity, and signal-to-noise ratio) through more advanced device assemblies and the integration of nanomaterials-based bio-interface materials (e.g. metal nanoparticles, and carbon nanotubes) as electrode surface modifiers [1]–[4].

Electrochemical glucose monitoring biosensors (i.e., glucometers) are of particular interest to this study. They have been the most growing medical devices with a market size of $12.8 Billion in 2019 [5]. Current research on electrochemical glucometers focuses on enhancing their reliability, stability, sensitivity, and portability while maintaining low cost [6]. In principle, there're two electrochemical glucose detection approaches; enzymatic and non-enzymatic. Enzymatic approaches employ glucose oxidase enzyme (GOx) as a recognition element. They work by oxidizing glucose molecules and the generation of detectable compounds such as O_2, CO_2, or H_2O_2. In this aspect, glucose oxidase breaks into gluconolactone, hydrogen, and oxygen when interacting with enzymatic sensors. The detection mechanism of the sensors depends on the concentrations of the original glucose on the surface of the sensor, which results in the oxidizing of glucose and presenting in typical current values in response to the concentration of the glucose. Although they have high specificity, which ultimately reflects in the overall device selectivity, there are still significant challenges in the development of GOx-based glucometers, namely (i) their sensitivity is degraded with time due to enzyme leaching, (ii) they suffer from low stability and short life-time; being a protein, GOx enzyme highly susceptible to environmental factors such as pH, chemical reagents, temperature, and humidity, and, (iii) reduction in high overpotentials.

Hence, these challenges have stimulated the research to develop more reliable electrochemical glucometers through an alternative non-enzymatic approach. In this approach, a more stable and reliable metal or metal oxide-based electrocatalytic media (e.g., Pt or CuO) is employed to oxidize glucose on the electrode surface directly. Several developments of non-enzymatic have reported enhanced sensitivity (e.g. 0.01 - 0.46 $\mu A\ mM^{-1}\ cm^{-2}$ [7], [8], fast response (e.g. 1 sec, [9]), and low-cost and high reproducibility ([10];[11]). However, when compared to enzymatic sensors, most of the reported sensors suffered from a short linear range (e.g., 0.5 – 7.5 mM, [12].), and low selectivity[12] due to the interference with other chemical components in whole mammalian blood such as ascorbic or uric acids. Hence, the most sought-after achievement for the next generation non-enzymatic glucometers is the improvement in the device selectivity, reliability, and sensitivity ([13]).

As such, several technologies have been investigated to develop the electrochemical reaction-based electrode surfaces in non-enzymatic glucometers including carbon-based materials (e.g. graphene, rGO, and CNT)[14], [15], which due to their remarkable electrical and physical/chemical properties, they have been widely investigated as electrochemical electrodes in various electrochemical biosensor applications [16], [17]

Accordingly, in this work, we have investigated and optimized the physio/chemical performance of a novel graphene/PtO/n-Si heterostructured electrode for non-enzymatic glucose biosensors with the primary objective of enhancing the linear detection range and reducing the interference between glucose and other chemicals in the whole blood in order to enhance selectivity. The critical challenge in this research is to achieve high selectivity, which maintaining, wide linear

Peer-reviewed version available at Sensors 2019, 20, 145; doi:10.3390/s20010145

range and low detection limit; this is carried out by optimizing the G/PtO film thickness and enhancing their interface. Therefore, for the first time, an ALD-grown Platinum oxide (PtO) was effectively employed as both a catalyst to grow graphene and an electrocatalytic agent for the oxidation of glucose and H_2O_2 molecules, respectively. Pt and PtO are considered as the strongest catalytic metals/metal oxides for glucose detection [18], [19]. However, there are some limitations associated with Pt/PtO sensors, including their degradation due to the adsorption of physiological solutions such as some uric and some amino acids [11,12,[22],17] hypothesized the advantage of using PtxCO1−x alloy nanoparticles and carbon as a support, with this alloy representing the enhancement of device selectivity toward glucose and linear response at different concentrations. Moreover, it avoids the competitive effects of fructose, uric acid, and ascorbic acid. Hence, in this work, graphene is also employed as both a protective and sieving layer to protect PtO film and further enhance sensor stability and selectivity, in addition, to due to its high electrical conductivity graphene-based electrodes contributed to the enhancement of device sensitivity.

Theoretical and experimental analyses revealed that G/PtO interface results in a carrier-free region where the two materials align in their fermi levels by charge transfer from graphene to Pt [21]. Graphene is p-doped because of fermi-level alignment, and I-V characteristics would show when applying a forward or reverse bias forms symmetric current because of electrons flow [12-20]. In addition, a depletion region is formed at the interface of PtO/Si due to the migration of carriers, which depends on the carrier distribution function and the concentration at the silicon surface.

We've further investigated the selectivity and charge transfer behavior using a Density Functional Theory (DFT) Model. The model findings were in line with the experimental results as the charge transfer of D-type glucose adsorbed on top of a graphene sheet resting on top of a Pt<111> substrate cut was noticed, as well as the direct adsorption of D-glucose on top of a Pt <111> substrate surface

Sensitivity enhancement by ~70-150% was observed by altering PtO and G layer thicknesses. All sensors structures have exhibited excellent selectivity when examined against whole blood components such as sodium chloride (NaCl), potassium chloride (KCl), urea extra pure, potassium, and phosphate monobasic (K_2PO_4). From this work, the results of the sensor showed an enhanced sensitivity in the sensor by changing the thickness of the PtO layer, as shown in the hysteresis analysis, selectivity, and cyclic voltammetry figures.

2. Materials and Methods

2.1. Chemicals

D-(+)- glucose monohydrate ($C_6H_{12}O_6.H_2O$), sodium phosphate monobasic dehydrate (H_6NaO_6P), sodium chloride (NaCl), and potassium chloride (KCl) were purchased from Sigma-Aldrich. Urea extra pure was obtained from Labchemie. Potassium phosphate monobasic K_2PO_4 was obtained from Aldrich Chem. Co. Phosphate buffer saline (pH=7.4) 0.1mM was prepared fresh for every experiment.

2.2. Device Fabrication

Starting from an N-type silicon wafer and then the deposition of a PtO thin film was performed by Atomic Layer Deposition (ALD) using Cambridge NanoTech Savannah ALD deposition system. The used precursors were Trimethyl (methylcyclopentadienyl) Pt (IV) with high purity O_2 used as an oxidizing agent. Deposition temperature was 275°C for 50 – 500 ALD-cycles to produce a PtO thin film with thickness ranging from 50 – 500Å, respectively. Subsequently, graphene bottom-up growth was done in Plasma Enhanced Chemical Vapor Deposition (PECVD) using Oxford Instruments, Plasmalab 100 PECVD System. The pressure was maintained at 1500 mTorr, and the chamber was heated from 195 – 600°C in a methane (CH_4) rich environment. High frequency 13.56 MHz and low frequency 380 kHz powers were varied to control the structure and thickness of the obtained graphene structure.

Peer-reviewed version available at *Sensors* **2019**, *20*, 145; doi:10.3390/s20010145

2.3. Morphological and Structural Characterization

Morphological characterization was obtained with a Field Emission Scanning Electron Microscope (FESEM) by Zeiss. X-ray Photo-electron Spectroscopy (XPS) characterization data were performed on K-alpha XPS from Thermo Scientific in the range of 1-1350eV to inspect the surface chemistry of the graphene. Raman spectra of the graphene thin film were obtained by Enwave Optronics Raman Spectroscopy (λ_{ex}=532nm, P=500mW, acquisition time=10s).

2.3. Testing Setup and Theoretical Modelling

The device was tested via a semiconductor parameter analyzer for Current-Voltage (I-V) and Current-Time (I-t) measurements to verify the working mechanism by using different glucose concentrations and observing the effect of different competitive solutions as discussed in section 3.2. The electrochemical analysis was obtained using Biologic Potentiostat for cyclic voltammetry and amperometry measurements to identify oxidation and reduction of glucose molecules on the electrode surface, as well as the electrochemical electron transfer process of glucose on the surface. In an attempt to investigate the change in charge distribution due to the presence of glucose molecules on the surface, density functional theory (DFT) using Quantum ESPRESSO was helpful in solving the Schrodinger equation and for studying charge density in the presence and absence of glucose.

2.4. Working principle

The working principle of the device depends on the oxidation of glucose molecules on the surface of the proposed heterostructured electrode due to the catalytic activity of PtO thin film. In addition, the breakdown of glucose molecules into gluconolactone and the formation of gluconic acid, hydrogen H_2, and electrons [26] as represented in Figure 1. Forward bias was applied to the Si terminal, and the current was measured from the graphene surface. The physisorption interaction between graphene and PtO (i.e., metal-semiconductor Schottky junction) resulted in a shift in the fermi-level position and p-doping of graphene.

PtO was chosen as a suitable candidate for two main reasons: its catalytic activity towards graphene growth and its catalytic activity towards glucose oxidation [25,26] Pt catalytic activity towards graphene growth was studied previously [Our Refs here] owing to the intense catalytic activity of PtO for CH_4 dissociation compared to Cu or Ni, and for its strong ability for H_2 dissociation [27–29]

Whereas, the electrocatalytic oxidation of D-glucose at the PtO surface is proposed to take multiple steps as follows: Graphene is considered an excellent supporter of electrochemical devices, as it enhances electrical conductivity, selectivity, stability, and sensitivity[2] Oxidation and reduction of glucose molecules result in the formation of gluconolactone and the release of electrons and H_2 as shown in Figure 1, and then the formation of gluconic acid [2]. Finally, the electrons from oxidation will start to cause variations in the Schottky barrier height.

As such, oxidation of glucose molecules on the surface structure changed the local electric field distribution and the variation in Schottky barrier height (SBH) in PtO/N-Si, resulting in detectable current changes due to molecule adsorption. Figure 1 illustrates the working principle of the structure in the presence and absence of glucose molecules on the device. As shown, in the absence of glucose, the fermi level of the graphene layers was aligned with the fermi level of PtO. With the presence of glucose molecules, fermi levels were aligned, and after applying bias on the silicon, the fermi levels started to shift due to the oxidation of glucose due to the liberating free electrons as a result of oxidation. This shift was noticed in the Schottky barrier height between G/PtO and Si. The shift in Fermi levels and the change in the barrier height can be correlated to the concentration of glucose with significant linearity.

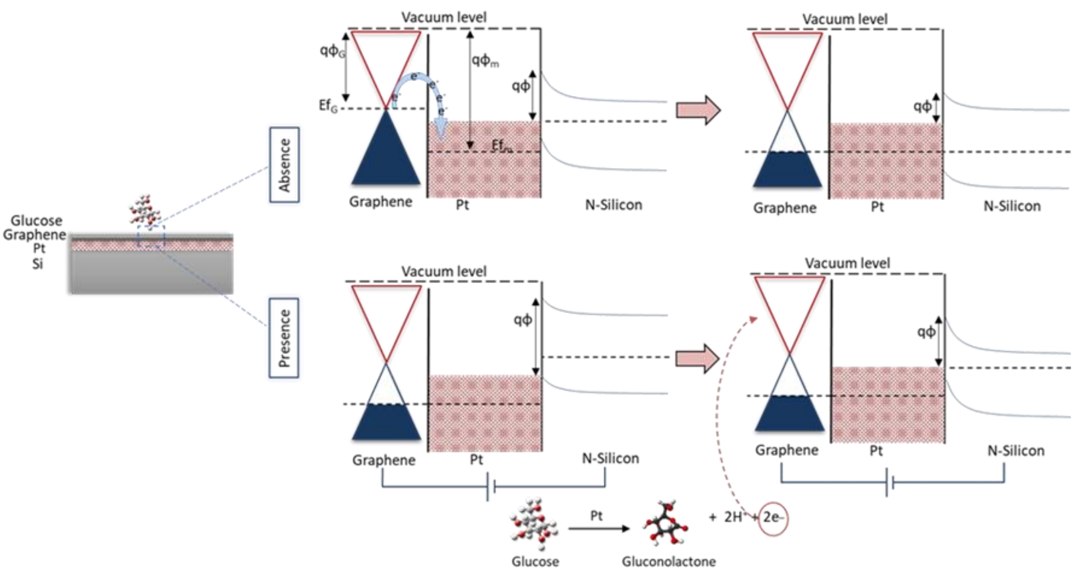

Figure 1. Graphical scheme for the working principle of the device

2.5. Theoretical Study

To gain more insight into the adsorption of D-glucose on top of graphene residing on a slab of PtO, density functional theory (DFT) simulations were performed. The PtO slab was formed by a (111) surface cut in a bulk PtO cubic system, forming a hexagonal substrate. The DFT calculations were carried out using the plane-wave basis set Quantum ESPRESSO (QE) [30] code. The optimized norm-conserving scalar relativistic [31,32] pseudopotentials (ONCV) were downloaded from PseudoDojo and developed by the University of California were used at the recommended plane-wave cut-off of 60 Ry. The Generalized Gradient Approximation (GGA) functional was used with the Perdew, Burke, and Ernzerhof (PBE) [33] parameterization for the exchange-correlation part in conjunction with the semi-empirical Grimme correction [34,35] with implementation in QE as a correction for the weak van der Waals (vdW) forces. Gaussian smearing of 0.03 Ry was applied. The Brillouin zone was sampled with 9x9x1 k-point mesh when the supercell was folded to the graphene's primitive unit cell. The calculational supercell had a vacuum set to≈20Å to eliminate any interaction between supercell repetitions in the z-direction. The slab cuts, as well as the supercell formation and transformation operations, were generated via the CIF2Cell utility code [36] and the Virtual NanoLab version 2016.1 from Quantum Wise A/S. The D-glucose structure was downloaded as an XYZ formatted structure file [37].

3. Results and Discussion

3.1. Morphological characterization

Figure 2 illustrates the XPS survey spectra of the graphene surface after 0, 50, and 100 sec etching of the surface. Three main peaks were resolved from this figure with binding energies of 75.08 eV for Pt, 285.08 eV for C, and 520.08 eV for O, respectively. It is observed that the peaks obtained indicating the existence of both graphene and PtO near the surface, which confirms the electrocatalytic/charge transfer detection principle outlined in the previous section.

Figure 3 illustrates the Raman spectrum of the graphene surface deposited at various deposition conditions with PtO film layer thickness of 5, 10, 30, 40 and 50 nm. The figure displays the graphene’s D, G, and 2D bands. The shift in the G band can be attributed to the PtO/graphene physisorption interaction [41]. Bonding between graphene and metallic atoms might affect the work function of graphene and the electronic band structure, and in our case the physisorption interaction between PtO/graphene might result in slight shifting in graphene’s fermi level. In our case, the work function of PtO is 5.98eV and graphene’s is 4.48eV. [42], [43].This interaction can be noticed in the shift in the Raman peaks .[40] Accordingly, shifts in the Raman D and G bands in 1324 cm^{-1}, 1574 cm^{-1},2692 cm^{-1}

were observed, respectively. FESEM was employed to investigate the morphology of PtO thin films on the n-Si surface and to measure its thickness. As shown in Figure 4, the orientation of PtO atoms on the surface of n-Si and the enhancement of the nucleation/growth of the PtO on the surface were directly related to the number of ALD cycles. A thin layer of PtO is formed on the surface of n-Si as shown in SEM images. In addition, as shown in Figure 4(f), the thickness of the PtO thin film is in the order of 50nm at 500 ALD-cycles.

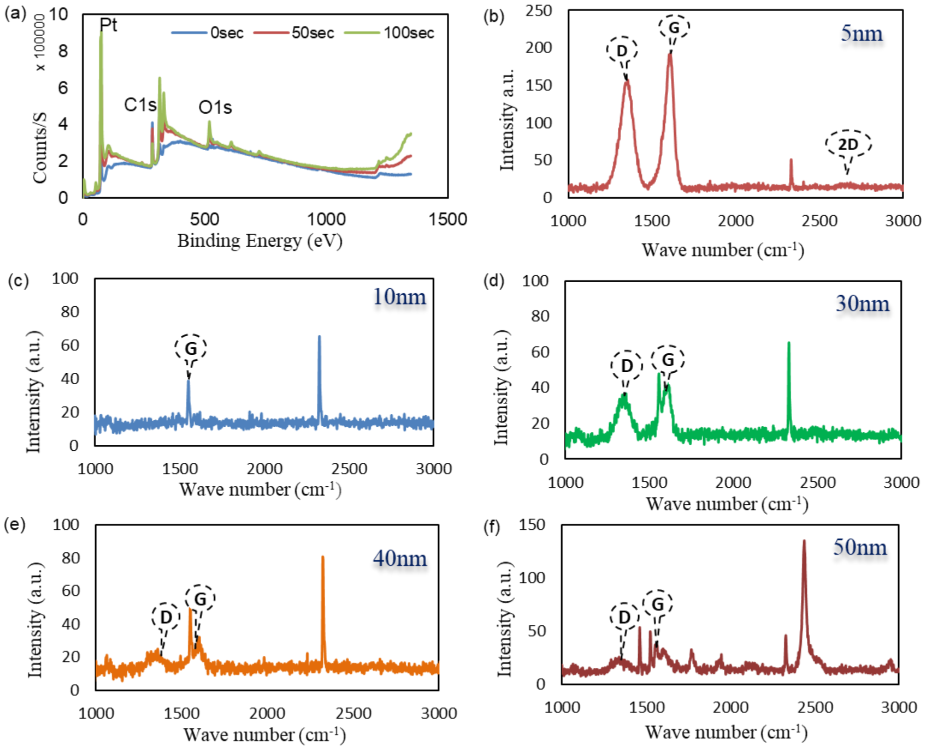

Figure 2 (a) XPS survey spectra on the surface of the graphene film after 10s, 30s, and 80s etching of the surface. RAMAN spectra of Graphene layers on top of different Pt thicknesses (b) 5, (c) 10, (d) 30, (e) 40, (f) 50nm film is in the range of 50nm deposited using 500 ALD cycles.

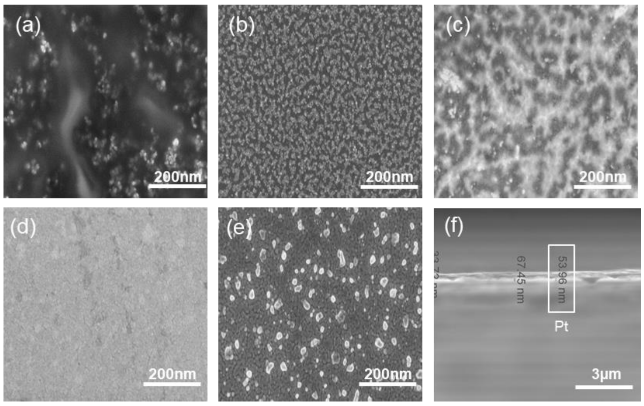

Figure 3. FESEM of Graphene layers on top of different Pt thicknesses (a) 5, (b) 10, (c) 30, (d) 40, (e) 50nm, (f) cross section of 50nm PtO

3.2. In-situ Sensitivity, Selectivity, and Linearity Tests

Using a graphene schottky diode, we tested different glucose concentrations to obtain the sensitivity of the device. The semiconductor parameter analyzer setup was used to investigate the response of the diode in the circuit to measure the charge difference due to glucose oxidation and the formation of gluconolactone and the subsequent H_2 adsorption on graphene surface, as well as the charge transfer in the opposite directions under forward bias. Moreover, a significant correlation was noticed between the output current and the concentration of the glucose. A 0.8-2μA difference was noticed in the case of 4-10mM glucose as shown in Figure 4 (a). In addition, the device showed no response in the presence of deionized water, sodium chloride, and urea which clarifies the sensitivity of the device towards glucose molecules. From these results, the sensitivity of the device is 0.2μA/mM.cm^2 which is comparable to recent sensitivity values in literature. While the device sensitivity is moderate as compared to the present carbon-based materials, the selectivity and linearity figures are among the highest in the non-enzymatic class.

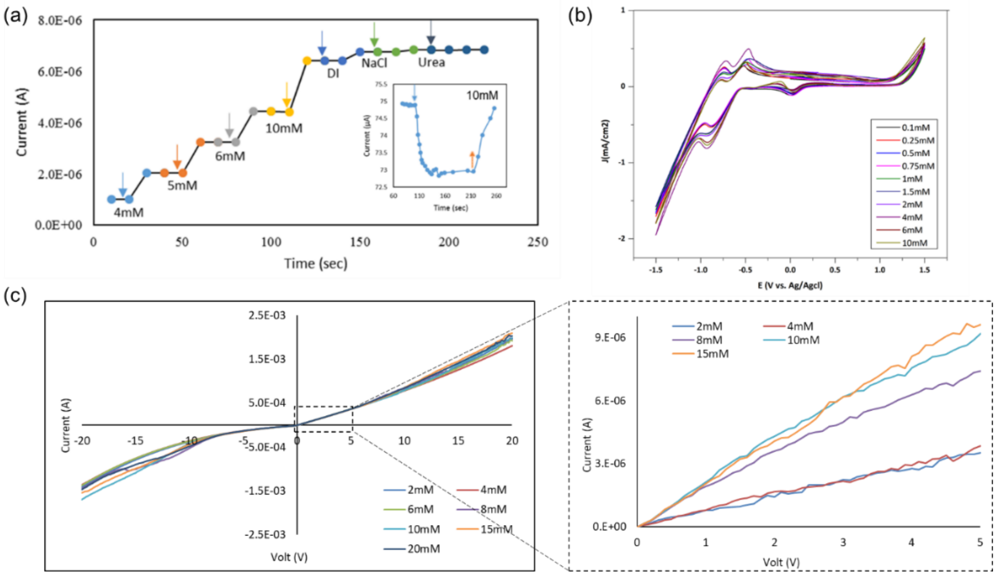

Figure 4 (a)Testing 4-10mM of glucose on Graphene/30nm Pt/N-Si, (b) Cyclic Voltammetry of different Glucose concentrations (0.1-10mM) using a Graphene/30nm PtO, (c) Testing DI, NaCl, and urea characteristics of the structure in presence of NaCl, Urea, Glucose and mixtures

Different glucose concentrations (0.1-1mM) in phosphate buffer saline (PBS) (pH=7.4) were tested on a biologic potentiostat for cyclic voltammetry which was conducted at (-1.5:1.5) mV with scan rate 20mV. Measurements included three electrode cells with Ag/AgCl as a reference electrode and a Pt sheet as a counter electrode. Nitrogen gas purging was carried out during the process to keep the surface active and stop any formation of oxide layers. As shown in Figure 4 (b) Oxidation and reduction peaks confirmed the formation of gluconolactone, gluconic acid molecules, free electrons, and dissociated H_2 on the surface of the device. Device sensitivity and its correlation to PtO film thickness were studied for different glucose concentrations 0.1-10mM using a Graphene/30nm PtO schottky diode by testing 4 mM glucose concentration on each PtO thicknesses as shown in Figure 5 (b), and (a). I-V characteristics of the device shows a potential difference between the different glucose concentrations from 2-20mM on 30 nm. It shows a consistency and significant difference

A selectivity test was obtained using a potentiostat and a parameter analyzer to test a 2.4 x 3 cm^2 sensor under 0.3 V bias in bare PBS and after adding different chemical solutions (i.e. sucrose, H_2O_2, KCl, NaCl, Na_2SO_4, and urea) as shown in Figure 6(c). It was noticed there was no response from the

Peer-reviewed version available at *Sensors* **2019**, *20*, 145; doi:10.3390/s20010145

device in the presence of the different solutions, and there was no blocking of the active sites. Figure 5 (c) illustrates the I-V characteristics of the structure in the presence of different solutions to check the selectivity. The results show that the responses of NaCl and urea, separate and together, are very small compared to the glucose readings. In addition, in Figure 10, the I-V characteristics of different glucose concentrations 2-20mM show the linearity of the response with a sweep bias between 5 to -5V.

3.2. Effect of PtO Thickness on Device Performance

Varying the PtO film thickness resulted in an enhancement in graphene growth due to the enhanced nucleation [30], [31]. By testing different PtO thicknesses with a fixed glucose concentration of 4mM, it was noticed that there was a strong correlation between the thickness and the enhanced catalytic activity of the device by increasing the oxidation rate and hence increasing output current/sensitivity, as shown in Figure 5 (a). An enhancement in sensitivity in the order more than 110 times as observed as the PtO film thickness was increased from 5-50 nm, respectively.

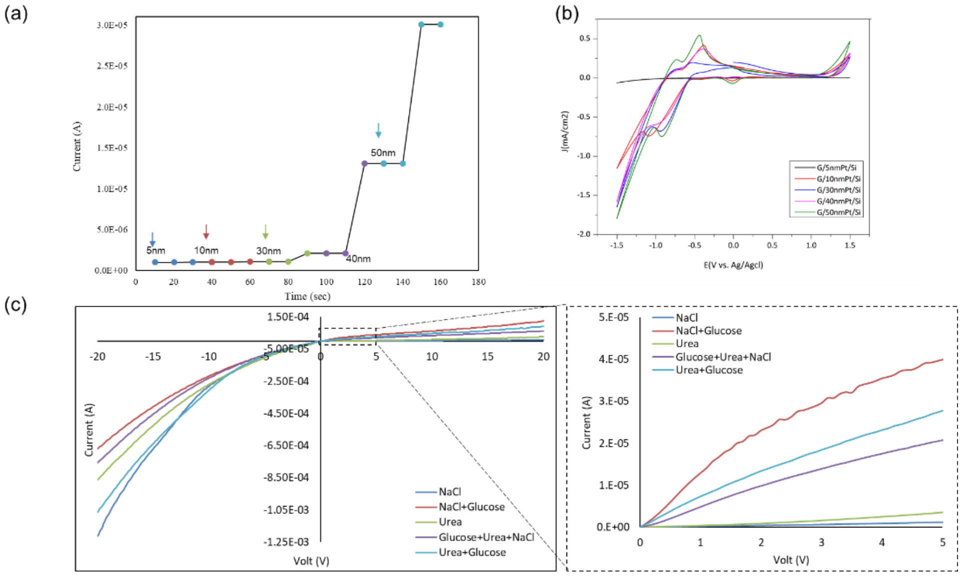

Figure 5 Testing 4mM glucose on (5-50nm) Pt, I-V characteristics of the presence of different glucose concentrations from 2-20mM (a) sweep voltage from -20 to 20V, (b) 0-5 V, Cyclic Voltammetry of different Glucose concentrations (a) testing 4mM on different Pt thicknesses

3.3. Device Reliability and Hysterisis Analysis

Figure 6 (a) illustrates the average reading of the device as 2 μA for 10mM glucose, where the blue arrows represent adding glucose on the sensor, and the red ones for removing them. The analysis, Figure 6 (a & b), shows the usability of the sensor for 12 rounds for 1.15 hours with standard deviation 0.5% which makes the device suitable for long-term studies.

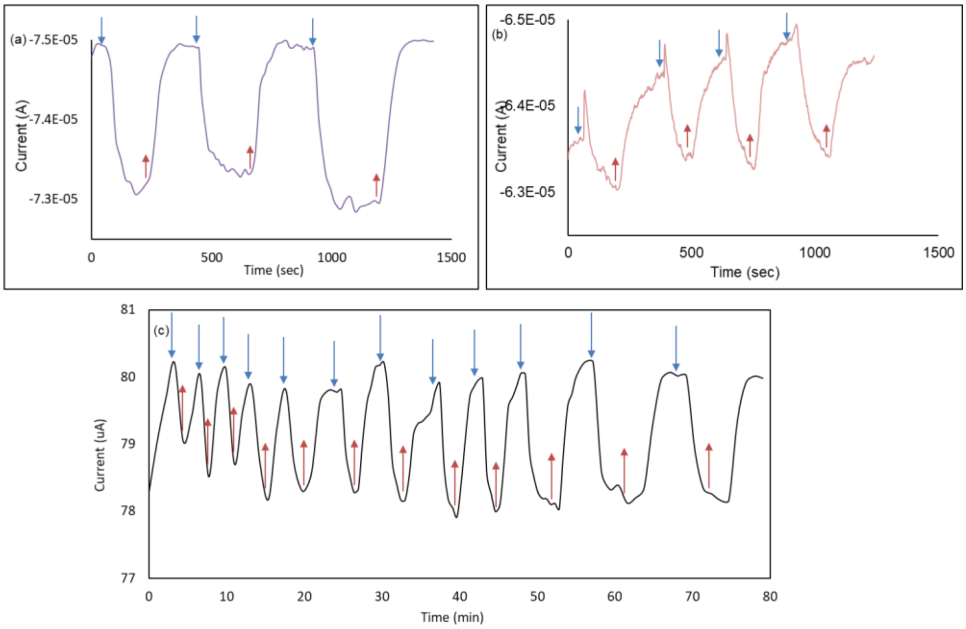

Figure 6 Response and Hysteresis Analysis (a) I-t measurements for 10mM on Graphene/30nmPt/N-Si device, (b) reproducibility test for 1h20mins using 10mM glucose on the same structure as in (a).

3.3. Theoretical Analysis

The sensing properties of graphene have been investigated for different species adsorbed on its surface [41–45]. Graphene's electronic structure properties and response to adsorbates were proven to change depending on the underlying substrate, as well as adsorbates existence on top [46–49]. The functionalized graphene response to D-glucose adsorbates on top was examined recently towards building a glucose biosensor device. Smith et. al, [49,50,51] had investigated graphene's humidity and CO_2 sensing behavior through visualizing charge transfer throughout the graphene sheet within the calculational supercell, where they analyzed the effect of water and CO_2 adsorbates on top of a graphene sheet. Similarly, in this work, the charge transfer of D-type glucose adsorbed on top of a graphene sheet resting on top of a Pt111 substrate cut was noticed, as well as the direct adsorption of D-glucose on top of a Pt <111> substrate surface.

Calculations were performed on two calculational setups, where the first was graphene relaxed on top of a Pt <111> substrate surface with the D-glucose structure relaxed on top of the graphene sheet, while the second was the Pt <111> substrate with the D-glucose structure relaxed directly on top of the Pt <111> substrate. All system components were relaxed where the graphene sheet recorded a spacing of 3.1Å above the Pt substrate, while the D-glucose recorded 3.5Å above the graphene sheet and 3.63Å above the Pt <111> substrate (the distance recorded between a z-coordinate value of a carbon atom in the graphene sheet and the mean z-value of the D-glucose structure). The resultant system setup is depicted in Figure 7 (a)

The electronic Charge Density Differences (CDDs) were calculated and extracted as 3D isosurface contour plots as depicted in Figure 7 <CDDs>. The changes in the electronic charge densities were defined as indicated in Equation 1. From the CDDs, the charge depletion regions dominated across the graphene sheet while charge accumulation regions were concentrated on the top layer of the Pt substrate within the supercell sans the D-glucose adsorbate on top (as depicted in the left panel of Figure 7 (b). Adding the glucose on top, the charge depletion regions along the

Peer-reviewed version available at *Sensors* **2019**, *20*, 145; doi:10.3390/s20010145

graphene sheet became thicker and associated with charge accumulation regions at the coordinates where glucose exists, while the charge accumulation regions alongside the top-most layer of the Pt substrate got thicker as well as depicted in the middle panel of CDDs Figure 7 (c).. Meanwhile, in the relaxed D-glucose on top of the Pt substrate system, alternating charge accumulation and depletion regions moving from the Pt substrate towards the D-glucose were observed.

Equation 1

$$\Delta\rho = \rho_{Pt-G-glucoe} - \rho_{Pt111} - \rho_{G} - \rho_{glucose}$$

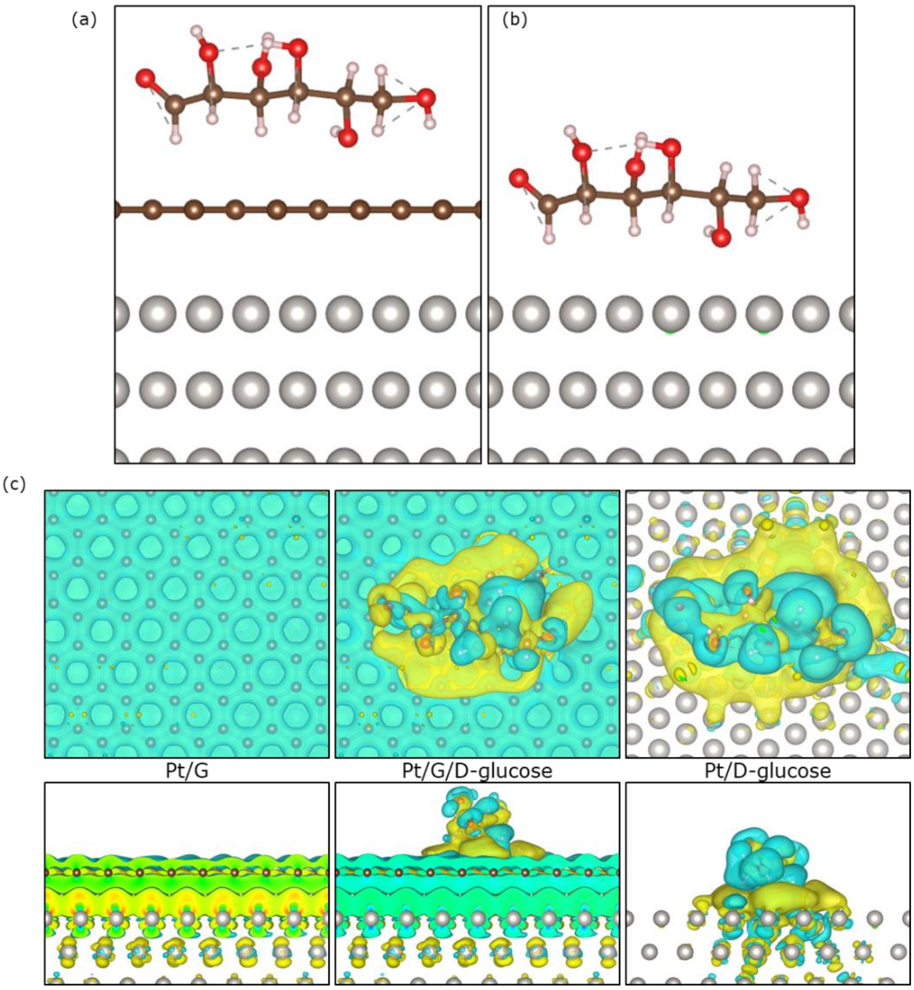

Figure 7 Systems setup, the left panel (a) depicts the adsorbed D-glucose on top of a relaxed graphene sheet on top of a Pt <111> substrate. The right panel (b) shows the relaxed D-glucose directly on top of the Pt111 substrate. The atoms are shown in spheres. where Pt atoms are rendered in grey, carbons in brown, oxygens in red, hydrogens in white, (c) Charge density difference contour plots (generated via VESTA package [VESTA]) for D-glucose on top of Pt <111> substrate and Pt111/Graphene combined system. The top subfigures are top views for the contours, while the bottom subfigures show the side views. The atoms are shown in spheres

5. Conclusion

In this paper, we discussed a new Graphene-heterostructured design and the applicability of using it for glucose level detection in diabetes monitoring. Fabrication and characterization techniques illustrated the working principle of the device by describing the changes in the Schottky barrier height. This was due to the presence of glucose molecules and the breakdown to gluconolactone due to the catalytic activity of Pt thin films. The presence of glucose molecules on the surface of the device resulted in a current that moves in the opposite direction to the applied bias (forward bias), with the difference between the two current values representing the concentration of glucose molecules. A selectivity test was obtained using different competitive solutions NaCl, KCl, sucrose, Na_2SO_4, and urea in two forms (1) separate and (2) mixed solutions to investigate the response of the device. It was noticed that there was a slight difference between the solutions, with a more noticeable difference when a droplet of glucose was added. An effect on Pt thickness was observed due to the presence of the same glucose concentration and due to the oxidation process. Density functional theory calculation results gave a qualitative explanation of the charges distributed across the graphene sheet within a system of platinum substrate and D-glucose molecules on top. Further analysis will investigate the presence of other molecules in the presence of bias on the system and will help in future efforts to further investigate the response of the device by quantum chemistry analysis.

Acknowledgments: The authors would like to acknowledge the financial support from the American University of Cairo through the AUC-Faculty Support Grants.

References

[1] M. Ferrari, Ed., BioMEMS and Biomedical Nanotechnology: VI: Biomedical & Biological Nanotechnology. V2: Micro/Nano Technology for Genomics and Proteomics. V3: Therapeutic Micro/Nanotechnology. V4: Biomolecular Sensing, Processing and Analysis. Springer US, 2006.

[2] X. Xie et al., “Enhancing the Nanomaterial Bio-Interface by Addition of Mesoscale Secondary Features: Crinkling of Carbon Nanotube Films To Create Subcellular Ridges,” ACS Nano, vol. 8, no. 12, pp. 11958–11965, Dec. 2014.

[3] M. Rahmati and M. Mozafari, “Biological Response to Carbon-Family Nanomaterials: Interactions at the Nano-Bio Interface,” Front. Bioeng. Biotechnol., vol. 7, Jan. 2019.

[4] A. Marino, G. G. Genchi, E. Sinibaldi, and G. Ciofani, “Piezoelectric Effects of Materials on Bio-Interfaces,” ACS Appl. Mater. Interfaces, vol. 9, no. 21, pp. 17663–17680, May 2017.

[5] “Global Blood Glucose Monitoring Market - Growth, Trends and Forecast (2019 - 2024).” [Online]. Available: https://www.mordorintelligence.com/industry-reports/global-blood-glucose-monitoring-market-industry. [Accessed: 30-Aug-2019].

[6] W.-C. Lee et al., “Comparison of enzymatic and non-enzymatic glucose sensors based on hierarchical Au-Ni alloy with conductive polymer,” Biosens. Bioelectron., vol. 130, pp. 48–54, Apr. 2019.

[7] J. H. Yuan, K. Wang, and X. H. Xia, “Highly Ordered Platinum-Nanotubule Arrays for Amperometric Glucose Sensing,” Adv. Funct. Mater., vol. 15, no. 5, pp. 803–809, 2005.

[8] H. Thabit et al., “Home use of closed-loop insulin delivery for overnight glucose control in adults with type 1 diabetes: a 4-week, multicentre, randomised crossover study,” Lancet Diabetes Endocrinol., vol. 2, no. 9, pp. 701–709, Sep. 2014.

[9] D. R. Powell et al., “LX4211 Increases Serum Glucagon-Like Peptide 1 and Peptide YY Levels by Reducing Sodium/Glucose Cotransporter 1 (SGLT1)–Mediated Absorption of Intestinal Glucose,” J. Pharmacol. Exp. Ther., vol. 345, no. 2, pp. 250–259, May 2013.

[10] L. Mei et al., “Non-enzymatic sensing of glucose and hydrogen peroxide using a glassy carbon electrode modified with a nanocomposite consisting of nanoporous copper, carbon black and nafion,” Microchim. Acta, vol. 183, no. 4, pp. 1359–1365, Apr. 2016.

[11] R. Shenoy, M. W. Tibbitt, K. S. Anseth, and C. N. Bowman, “Formation of Core–Shell Particles by Interfacial Radical Polymerization Initiated by a Glucose Oxidase-Mediated Redox System,” Chem. Mater., vol. 25, no. 5, pp. 761–767, Mar. 2013.

[12] S. Zhao et al., “α/β-Hydrolase domain-6-accessible monoacylglycerol controls glucose-stimulated insulin secretion,” Cell Metab., vol. 19, no. 6, pp. 993–1007, Jun. 2014.

[13] K. E. Toghill and R. G. Compton, “Electrochemical non-enzymatic glucose sensors:a perspective and an evaluation,” Int. J. Electrochem. Sci., vol. 5, no. 9, pp. 1246–1301, Sep. 2010.

[14] S.-Y. Kwon, H.-D. Kwen, and S.-H. Choi, “Fabrication of Nonenzymatic Glucose Sensors Based on Multiwalled Carbon Nanotubes with Bimetallic Pt-M (M = Ru and Sn) Catalysts by Radiolytic Deposition,” Journal of Sensors, 2012. [Online]. Available: https://www.hindawi.com/journals/js/2012/784167/. [Accessed: 07-Nov-2019].

[15] R. P. Tortorich, H. Shamkhalichenar, and J.-W. Choi, “Inkjet-Printed and Paper-Based Electrochemical Sensors,” Appl. Sci., vol. 8, no. 2, p. 288, Feb. 2018.

[16] Z. Bai et al., “Non-enzymatic electrochemical biosensor based on Pt NPs/RGO-CS-Fc nano-hybrids for the detection of hydrogen peroxide in living cells,” Biosens. Bioelectron., vol. 82, pp. 185–194, Aug. 2016.

[17] J.-J. Shi, W. Hu, D. Zhao, T.-T. He, and J.-J. Zhu, “Sonoelectrochemical synthesized RGO–PbTe composite for novel electrochemical biosensor,” Sens. Actuators B Chem., vol. 173, pp. 239–243, Oct. 2012.

[18] G. H. Wu, X. H. Song, Y. F. Wu, X. M. Chen, F. Luo, and X. Chen, “Non-enzymatic electrochemical glucose sensor based on platinum nanoflowers supported on graphene oxide.,” Talanta, vol. 105, pp. 379–385, Feb. 2013.

[19] A. Rengaraj et al., “Electrodeposition of flower-like nickel oxide on CVD-grown graphene to develop an electrochemical non-enzymatic biosensor,” J. Mater. Chem. B, vol. 3, no. 30, pp. 6301–6309, Jul. 2015.

[20] X. Yu, Y. Zhang, L. Guo, and L. Wang, “Macroporous carbon decorated with dendritic platinum nanoparticles: one-step synthesis and electrocatalytic properties,” Nanoscale, vol. 6, no. 9, pp. 4806–4811, Apr. 2014.

[21] M. Shafiei et al., “Platinum/Graphene Nanosheet/SiC Contacts and Their Application for Hydrogen Gas Sensing,” J. Phys. Chem. C, vol. 114, no. 32, pp. 13796–13801, Aug. 2010.

[22] H. J. Chun, Y. M. Park, Y. D. Han, Y. H. Jang, and H. C. Yoon, “Paper-based glucose biosensing system utilizing a smartphone as a signal reader,” BioChip J., vol. 8, no. 3, pp. 218–226, Sep. 2014.

[23] S. Chun, Y. Kim, H.-S. Oh, G. Bae, and W. Park, “A highly sensitive pressure sensor using a double-layered graphene structure for tactile sensing,” Nanoscale, vol. 7, no. 27, pp. 11652–11659, Jul. 2015.

[24] B. V. Zeghbroeck, Principles of Semiconductor Devices and Heterojunctions. Prentice Hall PTR, 2007.

[25] F. A. Chaves, D. Jiménez, A. W. Cummings, and S. Roche, “Model of the Electrostatics and Tunneling Current of Metal-Graphene Junctions and Metal-Insulator-Graphene Heterostructures,” ArXiv13090390 Cond-Mat, Sep. 2013.

[26] J.-S. Ye, B.-D. Hong, Y.-S. Wu, H.-R. Chen, and C.-L. Lee, “Heterostructured palladium-platinum core-shell nanocubes for use in a nonenzymatic amperometric glucose sensor,” Microchim. Acta, vol. 183, no. 12, pp. 3311–3320, Dec. 2016.

[27] S. Badhulika, R. K. Paul, Rajesh, T. Terse, and A. Mulchandani, “Nonenzymatic Glucose Sensor Based on Platinum Nanoflowers Decorated Multiwalled Carbon Nanotubes-Graphene Hybrid Electrode,” Electroanalysis, vol. 26, no. 1, pp. 103–108, Jan. 2014.

[28] C.-M. Seah, S.-P. Chai, and A. R. Mohamed, “Mechanisms of graphene growth by chemical vapour deposition on transition metals,” Carbon, vol. 70, pp. 1–21, Apr. 2014.

[29] Y.-P. Hsieh, M. Hofmann, and J. Kong, “Promoter-assisted chemical vapor deposition of graphene,” Carbon, vol. 67, no. Supplement C, pp. 417–423, Feb. 2014.

[30] M. Serry and M. A. Sakr, “Study of Flexoelectricity in Graphene Composite Structures,” MRS Adv., vol. FirstView, pp. 1–7, Aug. 2016.

Peer-reviewed version available at *Sensors* **2019**, *20*, 145; doi:10.3390/s20010145

[31] M. Serry and M. A. Sakr, “Modeling and experimental characterization of flexible graphene composite strain sensors,” in 2016 IEEE SENSORS, 2016, pp. 1–3.

[32] K. Tian, M. Prestgard, and A. Tiwari, “A review of recent advances in nonenzymatic glucose sensors,” Mater. Sci. Eng. C, vol. 41, pp. 100–118, Aug. 2014.

[33] P. Giannozzi et al., “QUANTUM ESPRESSO: a modular and open-source software project for quantum simulations of materials,” J. Phys. Condens. Matter Inst. Phys. J., vol. 21, no. 39, p. 395502, Sep. 2009.

[34] D. R. Hamann, “Optimized norm-conserving Vanderbilt pseudopotentials,” Phys. Rev. B, vol. 88, no. 8, p. 085117, Aug. 2013.

[35] M. Schlipf and F. Gygi, “Optimization algorithm for the generation of ONCV pseudopotentials,” Comput. Phys. Commun., vol. 196, pp. 36–44, Nov. 2015.

[36] J. P. Perdew, K. Burke, and M. Ernzerhof, “Generalized Gradient Approximation Made Simple,” Phys. Rev. Lett., vol. 77, no. 18, pp. 3865–3868, Oct. 1996.

[37] S. Grimme, “Semiempirical GGA-type density functional constructed with a long-range dispersion correction,” J. Comput. Chem., vol. 27, no. 15, pp. 1787–1799, Nov. 2006.

[38] V. Barone, M. Casarin, D. Forrer, M. Pavone, M. Sambi, and A. Vittadini, “Role and effective treatment of dispersive forces in materials: Polyethylene and graphite crystals as test cases,” J. Comput. Chem., vol. 30, no. 6, pp. 934–939, Apr. 2009.

[39] T. Björkman, “CIF2Cell: Generating geometries for electronic structure programs,” Comput. Phys. Commun., vol. 182, no. 5, pp. 1183–1186, May 2011.

[40] A. Gilbert, IQmol is an open source molecular editor and visualization package. 2017.

[41] G. Giovannetti, P. A. Khomyakov, G. Brocks, V. M. Karpan, J. van den Brink, and P. J. Kelly, “Doping Graphene with Metal Contacts,” Phys. Rev. Lett., vol. 101, no. 2, p. 026803, Jul. 2008.

[42] B. H. Chu et al., “Hydrogen detection using platinum coated graphene grown on SiC,” Sens. Actuators B Chem., vol. 157, no. 2, pp. 500–503, Oct. 2011.

[43] A. Rochefort, D.-Q. Yang, and E. Sacher, “Stabilization of platinum nanoparticles on graphene by non-invasive functionalization,” Carbon, vol. 47, no. 9, pp. 2233–2238, Aug. 2009.

[44] K. S. Subrahmanyam, A. K. Manna, S. K. Pati, and C. N. R. Rao, “A study of graphene decorated with metal nanoparticles,” Chem. Phys. Lett., vol. 497, no. 1–3, pp. 70–75, Sep. 2010.

[45] T. Kuila, S. Bose, P. Khanra, A. K. Mishra, N. H. Kim, and J. H. Lee, “Recent advances in graphene-based biosensors,” Biosens. Bioelectron., vol. 26, no. 12, pp. 4637–4648, Aug. 2011.

[46] Y. Dan, Y. Lu, N. J. Kybert, Z. Luo, and A. T. C. Johnson, “Intrinsic Response of Graphene Vapor Sensors,” Nano Lett., vol. 9, no. 4, pp. 1472–1475, Apr. 2009.

[47] F. Chekin et al., “Reduced Graphene Oxide Modified Electrodes for Sensitive Sensing of Gliadin in Food Samples,” ACS Sens., vol. 1, no. 12, pp. 1462–1470, Dec. 2016.

[48] J. Yang, T. J. Kwak, X. Zhang, R. McClain, W.-J. Chang, and S. Gunasekaran, “Digital pH Test Strips for In-Field pH Monitoring Using Iridium Oxide-Reduced Graphene Oxide Hybrid Thin Films,” ACS Sens., vol. 1, no. 10, pp. 1235–1243, Oct. 2016.

Peer-reviewed version available at *Sensors* **2019**, *20*, 145; doi:10.3390/s20010145

[49] E. C. Anota, A. T. Soto, and G. H. Cocoletzi, “Studies of graphene–chitosan interactions and analysis of the bioadsorption of glucose and cholesterol,” Appl. Nanosci., vol. 4, no. 8, pp. 911–918, Nov. 2014.

[50] T. O. Wehling, A. I. Lichtenstein, and M. I. Katsnelson, “First-principles studies of water adsorption on graphene: The role of the substrate,” Appl. Phys. Lett., vol. 93, no. 20, p. 202110, Nov. 2008.

[51] A. D. Smith et al., “Toward effective passivation of graphene to humidity sensing effects,” in 2016 46th European Solid-State Device Research Conference (ESSDERC), 2016, pp. 299–302.

[52] A. D. Smith et al., “Resistive graphene humidity sensors with rapid and direct electrical readout,” Nanoscale, vol. 7, no. 45, pp. 19099–19109, Nov. 2015.

[53] K. Elgammal, H. W. Hugosson, A. D. Smith, M. Råsander, L. Bergqvist, and A. Delin, “Density functional calculations of graphene-based humidity and carbon dioxide sensors: effect of silica and sapphire substrates,” Surf. Sci., vol. 663, pp. 23–30, Sep. 2017.

[54] A. D. Smith et al., “Resistive graphene humidity sensors with rapid and direct electrical readout,” Nanoscale, vol. 7, no. 45, pp. 19099–19109, Nov. 2015.

[55] A. D. Smith et al., “Graphene-based CO2 sensing and its cross-sensitivity with humidity,” RSC Adv., vol. 7, no. 36, pp. 22329–22339, Apr. 2017.